

---

AI translation · View original & related papers at  
[chinarxiv.org/items/chinaxiv-202506.00048](https://chinarxiv.org/items/chinaxiv-202506.00048)

---

# Numerical Simulation of Pressure Boundary Failure Accident in Lead-Bismuth Eutectic-Supercritical Carbon Dioxide Printed Circuit Heat Exchangers

**Authors:** Huang, Mr. Xi, Lixiang Zhang, Huang, Mr. Yuxin, Chen, Prof. Hongli, Zhang, Mr. Kefan, Chen, Prof. Hongli

**Date:** 2025-05-26T22:08:08+00:00

## Abstract

Due to its excellent heat transfer performance and compact structure, the printed circuit heat exchanger (PCHE) has become the mainstream heat exchange equipment between the secondary circuit of the supercritical carbon dioxide Brayton cycle and the primary circuit of the lead-cooled fast reactor. During the operation of the Lbe-SCO<sub>2</sub> PCHE, the huge pressure difference between the cold side (high pressure S-CO<sub>2</sub>) and the hot side (atmospheric pressure lead-bismuth eutectic) combined with the corrosion characteristics of the lead-bismuth eutectic could lead to the failure of the PCHE pressure boundary, potentially resulting in CO<sub>2</sub> leakage into the primary circuit. This study used the CFD software ANSYS Fluent to numerically simulate the PCHE pressure boundary failure accident. The feasibility of the analysis method is verified by decomposing the complex accident conditions into typical characteristic conditions for experimental simulation verification. The results show that during the accident transient process, the pressure in the hot channel initially exhibits cyclic fluctuations, rising sharply within 0.1ms and then gradually stabilizing; while the pressure in the cold channel remains essentially unchanged at the operating pressure. The simulation revealed that after 15ms after the accident, large quantities of carbon dioxide were detected at the inlet and outlet of the hot side, indicating a risk of intrusion of the secondary circuit's working medium into the reactor.

## Full Text

### Preamble

Numerical Simulation of Pressure Boundary Failure Accident in the Lead-Bismuth Eutectic-Supercritical Carbon Dioxide Printed Circuit Heat Exchanger

Xi Huang,<sup>1</sup> Li-Xiang Zhang,<sup>1</sup> Yu-Xin Huang,<sup>1</sup> Ke-Fan Zhang,<sup>1</sup> and Hong-Li Chen<sup>1,\*</sup> <sup>1</sup>School of Nuclear Science and Technology, University of Science and Technology of China, Hefei, Anhui, 230026, China

Due to its excellent heat transfer performance and compact structure, the printed circuit heat exchanger (PCHE) has become the mainstream heat exchange equipment between the secondary circuit of the supercritical carbon dioxide Brayton cycle and the primary circuit of the lead-cooled fast reactor. During operation of the LBE- $\text{SCO}_2$  PCHE, the enormous pressure difference between the cold side (high-pressure  $\text{S-CO}_2$ ) and the hot side (atmospheric-pressure lead-bismuth eutectic), combined with the corrosion characteristics of the lead-bismuth eutectic, could lead to failure of the PCHE pressure boundary, potentially resulting in  $\text{CO}_2$  leakage into the primary circuit. This study employs the CFD software ANSYS Fluent to numerically simulate the PCHE pressure boundary failure accident. The feasibility of the analysis method is verified by decomposing the complex accident conditions into typical characteristic conditions for experimental simulation verification. The results show that during the accident transient process, the pressure in the hot channel initially exhibits cyclic fluctuations, rising sharply within 0.1 ms and then gradually stabilizing, while the pressure in the cold channel remains essentially unchanged at the operating pressure. Simulation reveals that after 15 ms following the accident, large quantities of carbon dioxide were detected at the inlet and outlet of the hot side, indicating a risk of intrusion of the secondary circuit's working medium into the reactor.

### Introduction

The supercritical  $\text{CO}_2$  ( $\text{S-CO}_2$ ) Brayton cycle power generation system has become an ideal energy conversion solution for Generation IV nuclear reactors due to its significant advantages, such as compact equipment size, high thermal efficiency, and operational flexibility [1]. The lead-cooled fast reactor (LFR), as one of the most promising reactor types in Generation IV reactors, with its compact structure, small volume, and excellent thermal efficiency, perfectly matches the advantages of the  $\text{S-CO}_2$  Brayton cycle system [2].

The printed circuit heat exchanger (PCHE) offers high heat transfer capacity and small mass and size, making it the most widely used heat exchanger in the  $\text{S-CO}_2$  Brayton cycle [3]. As the pressure boundary between the primary and secondary circuits, the lead-bismuth eutectic (LBE)- $\text{S-CO}_2$  heat exchanger faces a significant pressure difference between liquid lead-bismuth and supercritical  $\text{CO}_2$ . This makes the safety issues arising from pressure boundary failure and

the resulting leakage non-negligible. Potential pressure boundary failure in the heat exchanger will cause supercritical CO<sub>2</sub> on the cold side to leak to the hot side and pressurize the system, which will threaten the structural integrity of the heat exchanger itself and its related systems. It is necessary to evaluate the boundary failure accident to confirm its impact on safety.

Currently, there are no direct experiments on the contact between liquid lead-bismuth and carbon dioxide, and very few experiments have been conducted on the contact between carbon dioxide and liquid metals. Jae-Hyuk Eoh et al. [4] conducted mixing experiments of S-CO<sub>2</sub> and sodium to analyze the mixing of the two substances due to the failure of the boundary conditions of the PCHE heat exchanger, and obtained the reaction models of these two substances and the kinetic parameters of the different reaction zones. Naoyuki Kisohara et al. [5] investigated the effect of S-CO<sub>2</sub> leakage from the PCHE of SFR to the sodium pipeline on the pressure increase and heat transfer performance at the primary circuit. The results showed that the leakage of CO<sub>2</sub> did not have a significant effect on the core and the boundary of the primary circuit due to the small volume of the single runner in the PCHE. Only studies of CO<sub>2</sub> exposure to sodium have been conducted, and there are no studies of LBE/Pb. Compared with SFR with intermediate loops, boundary condition failure accidents in LFR may directly affect core safety. The main difference between lead-bismuth eutectic and sodium is chemical stability. At operating temperatures, liquid lead-bismuth eutectic has relatively low chemical reaction activity and will not undergo vigorous chemical reactions with supercritical carbon dioxide.

Based on the ANSYS Fluent numerical simulation platform, this study aims to investigate the pressure wave propagation characteristics of a lead-bismuth eutectic-supercritical carbon dioxide (LBE-SCO<sub>2</sub>) printed circuit heat exchanger (PCHE) under a boundary condition failure accident. By decomposing the accident characteristics, the complex accident scenario is divided into typical transient processes, and the reliability of the numerical model is verified by comparing with experimental data. The study focuses on the propagation characteristics and evolution laws of pressure waves in the piping system during the accident transient process and analyzes the leakage characteristics. The migration and diffusion behavior of the leaked working fluid in the circuit was preliminarily assessed to evaluate the risk of CO<sub>2</sub> leakage to the reactor core.

## II. Model Validation

The boundary failure accident in an LBE-SCO<sub>2</sub> printed circuit heat exchanger (PCHE) can be characterized as follows: A fracture occurs in the solid region between the cold and hot channels, creating a connection that allows high-pressure CO<sub>2</sub> to enter the low-pressure lead-bismuth eutectic (LBE) channel. When the accident occurs, high-pressure S-CO<sub>2</sub> flows into the hot channel, undergoes transcritical depressurization, and transitions from a supercritical to a gaseous state. The resulting pressure wave propagates through the liquid LBE. However, there is currently very limited information available for such design considera-

tions. For the boundary failure accident analyzed in this study, the following assumptions are adopted:

- Supercritical carbon dioxide is chemically relatively inert at high temperatures and pressures. It is generally accepted that dry pure S-CO<sub>2</sub> fluids are stable at lower temperatures (<400 °C) and have a very low probability of reacting with metal parts in contact (pressure vessels, piping, etc.) [6].
- The disappearance of surface tension in supercritical fluids eliminates the stratification phenomenon between liquid and gas phases [7]. When S-CO<sub>2</sub> comes into contact with liquid metals, the surface tension of the liquid metal plays a dominant role.

In this paper, the boundary failure accident characteristics are divided into the following two points, with corresponding experimental validations conducted to evaluate the feasibility of the simulation methodology: - Transcritical depressurization analysis of supercritical carbon dioxide - Pressure wave analysis of gas injection into liquid metal

#### **A. Verification of the Supercritical Carbon Dioxide Transcritical Depressurization Model**

To investigate the depressurization characteristics of S-CO<sub>2</sub>, Gebbeken [8] performed depressurization experiments on the top of a S-CO<sub>2</sub> container, focusing particularly on flashing scenarios during pressure release. The study obtained comprehensive data on axial fluid temperature distribution, transient pressure evolution, and void fraction dynamics along the vessel's central axis, while systematically analyzing the influence of initial parameters on these characteristics. Wang et al. [9] conducted vessel depressurization experiments with S-CO<sub>2</sub> using nozzles of varying sizes under different initial temperature and pressure conditions. Their observations revealed that the initial temperature directly influences the occurrence of phase transition. Guo et al. [10] conducted experiments on the depressurization of industrial-scale pipelines with S-CO<sub>2</sub> and observed gas-liquid and gas-solid phase transition phenomena during the process.

In terms of numerical simulation, Ming et al. [11] established a transient characteristic model for the S-CO<sub>2</sub> discharge inside a pressure vessel based on Mod- elica. The program's flow rate and pressure calculation results were in good agreement with experimental data. Liu [12] used Fluent to conduct numerical simulations and analyses of the near-field jet and far-field shockwave structure of S-CO<sub>2</sub> leakage, utilizing the PR equation of state. Li [7] conducted a numerical simulation study on the free expansion jet process in small-scale supercritical leakage near-field using a self-developed two-step Lax-Wendroff (L-W) algorithm, with parallel experimental data comparison for validation. The thermodynamic parameters of CO<sub>2</sub> were calculated using the RK equation of state.

The transcritical depressurization phenomenon of supercritical carbon dioxide can be summarized into two types:

**1. Single-Phase Transcritical Depressurization** When the initial temperature is higher than the pseudo-critical temperature, the depressurization process maintains gaseous phase throughout without phase transition.

**2. Phase-Transition Transcritical Depressurization** When the initial temperature is lower than the pseudo-critical temperature, the fluid first depressurizes from the supercritical state into the saturation region, transitioning to liquid phase (gas-liquid two-phase depressurization). The saturated liquid then undergoes flash evaporation into gaseous state. With continued pressure reduction, the saturated liquid fully transitions to gas phase, resuming single-phase depressurization. If the temperature continues to drop during the flash evaporation process, liquid droplets solidify into dry ice [13]. After flash evaporation,  $\text{CO}_2$  exists in both gas and solid phases.

The pseudocritical temperature is as shown in Eq. (1) [14]:

$$T_{pc} = -122.6 + 6.124p - 0.1657p^2 + 0.01773p^{2.5} - 0.0005608p^3,$$

where the pseudocritical temperature  $T_{pc}$  is in  $^{\circ}\text{C}$  and the pressure  $p$  is in bar.

For the LBE- $\text{SCO}_2$  printed circuit heat exchanger, the system operates at 550-800 K with a cold-side working pressure of 20 MPa and hot-side at atmospheric pressure. During depressurization events within the 20 MPa range, the temperature consistently remains significantly above the pseudo-critical temperature. Consequently, when boundary failure accidents occur, the supercritical  $\text{CO}_2$  undergoes single-phase depressurization. Considering the nonlinear changes in the thermophysical properties of transcritical fluids, it is necessary to introduce the real gas equations of state (EOS), such as SRK, PR and other equations of state, which provide high accuracy for the thermodynamic parameters of supercritical fluids [15].

In this paper, the optimal equation of state for transcritical  $\text{CO}_2$  simulation is determined by numerical modeling and comparative analysis of experimental data. Meanwhile, the turbulence models commonly used in S- $\text{CO}_2$  CFD calculations, such as SST  $k-\omega$  and SST  $k-\omega$  low-Re [16], are mainly used for heat transfer analysis. Their applicability to transcritical depressurization conditions requires further validation. Therefore, the selection of turbulence models for the depressurization case is further investigated based on the selection of the equation of state. The main turbulence models in CFD currently include  $k-$ ,  $k-\omega$ , Reynolds stress, LES models, etc. Due to the poor convergence of the Reynolds stress model and the high computational cost of the LES model, as well as the unsuitability of the standard  $k-$  model for simulations involving near-wall flows, the selection is narrowed down to the  $k-\omega$  model and other  $k-$  variants.

## 1. Numerical Simulation of $\text{CO}_2$ Depressurization in a Short Pipe

To verify the state equation and turbulence model, the experiments of Liu et

al. [17] were selected. They conducted short-tube blowdown experiments with R744 refrigerant ( $\text{CO}_2$ ) to investigate its transcritical flow characteristics. The experimental setup is illustrated in Fig. 2 [FIGURE:2]. The pipe has a length of 12.92 mm and an inner diameter of 1.35 mm. The copper tube diameter is 7 mm. Using pressure inlet and outlet as boundary conditions as shown in Table 1, the same monitoring points as in the experiment were established to monitor the pressure. Based on the inlet and outlet pressures, the specific heat capacities at 9.02 MPa, 6.3 MPa and 3.53 MPa were selected for calculation, as shown in Fig. 4 [FIGURE:4] and Fig. 5 [FIGURE:5]. It can be observed that the closer the properties are to the inlet conditions, the better the simulation matches the experimental values, regardless of the turbulence model or EOS selected. Therefore, this study defines the specific heat capacity based on the initial pressure.

The simulated values were compared with the experimental values and the maximum as well as average errors are shown in Table 2. According to the error analysis, there was no significant difference between the four equations of state in this experimental simulation except for the ideal gas equation. This is because the ideal gas equation is not applicable to high temperature and pressure conditions. Among the four equations of state, the maximum and average errors of the PR and RK EOS are very small. Similarly, the turbulence model has little effect on this simulation. The simulation using SST  $k-\omega$  low-Re and Realizable  $k-\epsilon$  models are in good agreement with the experiment.

**2. Numerical Simulation of  $\text{CO}_2$  Depressurization in Vessel** To further evaluate the applicability of the S- $\text{CO}_2$  equation of state and turbulence model, a different experiment from the short tube depressurization was chosen. This section presents simulation verification of the S- $\text{CO}_2$  vessel depressurization experiments conducted by Wang et al. [9]. Two of the experiment conditions were selected, and the experiment conditions are summarized in Table 3. The experimental facility is shown in Fig. 8 [FIGURE:8].

Fig. 10 FIGURE:10 and Fig. 10(b) show the pressure variations calculated using the SST  $k-\omega$  Low-Re turbulence model for different specific heat capacities. The results are consistent with the conclusions drawn in section II A 1: the closer to the initial state, the better the agreement with the experimental values. Further error analysis of the experimental and simulated values is shown in Table 4 and Table 5. The variation of pressure over time with different nozzle sizes is shown in Fig. 11 [FIGURE:11] and Fig. 12 [FIGURE:12]. Based on the error analysis, for the turbulence model, regardless of the chosen equation of state (EOS), the SST  $k-\omega$  Low-Re model demonstrates outstanding applicability in the transcritical depressurization of S- $\text{CO}_2$  simulation. In terms of the equation of state, the Peng-Robinson (PR) equation shows reliable performance across all tested turbulence models. Therefore, in this paper, the SST  $k-\omega$  low-Re model is used as the turbulence model, and the PR equation of state is chosen for the thermophysical property calculation of S- $\text{CO}_2$ .

## B. Validation of the Gas Injection Model for Liquid Metal

The SST  $k-\omega$  low-Re turbulence model was selected for numerical simulation based on section II A 1. However, whether this turbulence model is suitable for studying pressure wave propagation in liquid metals still requires further verification. To assess the model's reliability, a gas injection experimental simulation was conducted. Currently, experiments on liquid lead-bismuth eutectic are more focused on lead-water reactions, while gas-liquid metal interaction experiments primarily focus on bubble dynamics. The injection of high-pressure water differs fundamentally from gas injection: water undergoes flash evaporation and phase change, whereas gas does not, leading to completely different pressure wave generation mechanisms.

For gas injection experiments, M. Utili et al. [18] conducted tests on helium gas impacting liquid lead-lithium (PbLi) to study IN-BOX LOCA, using Relap5 to analyze the propagation of pressure waves. Zhang et al. [19] investigated IN-BOX LOCA by injecting helium gas into liquid lead-lithium (PbLi) and performed pressure wave propagation analysis using Fluent [20]. To study the steam generator tube rupture (SGTR) of fast reactors, M V Alekseev et al. [21] used argon gas injection into the Rose's alloy experiment to observe pressure wave dynamics.

As there are currently no experiments on the contact between supercritical carbon dioxide and liquid metal, this section selects the experiment of M V Alekseev et al. [21] for simulation to verify the correctness of the model. The test section and simulation model of the experiment are shown in Fig. 13 [FIGURE:13]. In this paper, the Mixture model with moderate accuracy and computational cost was chosen as the multiphase flow model. In the selection of the drag force model, Zhang et al. [22] investigated the rising behavior of single bubbles in gallium indium tin alloy, and found that the Grace model and the Tomiyama model had smaller errors compared with the experimental values. Qing [23] simulated and analyzed the rising process of argon in gallium-indium-tin alloy, and found that the Tomiyama model showed better agreement with the experimental values. Chen [24] conducted numerical simulations of bubbles of different sizes rising in liquid lead. The results indicate that the Tomiyama model provides the best prediction for the terminal rising velocity of the bubbles. Thus, the Tomiyama model is selected as the trailing force model in Fluent.

Rose's metal consists of 50% bismuth, 25–28% lead and 22–25% tin by weight. The initial temperature of the experiment is 408 K, at atmospheric pressure. The argon gas injection pressure is 300 kPa, and the temperature is at room temperature. The Tait equation of state is used to describe the changes in density and sound speed of the liquid metal, as defined by the UDF, as shown in Eq. (2) and Eq. (3).

$$\rho = \rho_0 \frac{BS}{BS - (P - P_0)} \quad c = \sqrt{\frac{BS}{\rho_0} \frac{P - P_0}{\rho}}$$

where  $\rho$  is the current density,  $\rho_0$  is the reference density,  $P$  is the current pressure,  $P_0$  is the reference pressure,  $BS$  is the bulk modulus, and  $c$  is the local sound speed.

Pressure monitoring was conducted on sensor 1 as shown in Fig. 13, and the calculated values by Fluent are shown in Fig. 14 [FIGURE:14]. Although there is a certain difference between the simulated values and the experimental values at the peak, the overall trend is consistent. Moreover, the simulation in this study is closer to the experimental values compared to the results by M V Alekseev et al. using OpenFoam [21]. Therefore, it can be concluded that the method in this study is capable of simulating the pressure wave analysis of liquid metal and gas contact. These models will be used in the simulation of the pressure boundary failure accident of PCHE.

### III. Simulation Models

To simulate the potential pressure boundary failure accident of PCHE, the Sustainable Modular Mobile Enhanced Reactor (SUMMER) developed by the University of Science and Technology of China was used as the primary circuit [26]. Core design parameters are listed in Table 6. The secondary circuit is supercritical carbon dioxide Brayton cycle. The parameters of the printed circuit heat exchanger are shown in Table 7, and the steady-state operation parameters of the PCHE heat exchange unit are provided in Table 8.

When a pressure boundary failure accident occurs, it is assumed that the rupture occurs in the middle of the channel, and a straight-line crack forms, connecting the hot and cold channels through this crack. The cross-section of the rupture is a square with a side length of 0.1 mm, as shown in Fig. 17 [FIGURE:17]. Due to the short simulation time, the heat transfer between the hot and cold channels is neglected in this study. The solid domain is also ignored in the modeling, and the computational domain is shown in Fig. 18 [FIGURE:18].

The boundary conditions for both the hot and cold channels are set as pressure inlet/outlet, with values set as the operating pressure. The initial values are the temperatures, pressures and velocities at the rupture planes of the cold and hot channels during the steady state. Monitoring points are established respectively in the cold and hot aisles, as shown in Fig. 19 [FIGURE:19]. Among them, point A is located directly above the breach in the hot aisle, points B and C are at the 1/4 length position of the hot aisle and near the entrance and exit respectively, and points D, E, and F correspond to the same positions in the cold channel.

### IV. Pressure Analysis of Pressure Boundary Failure Accidents in PCHE

#### A. Grid Independence Verification

In this study, ICEM is employed for grid generation, with grids near the rupture zone encrypted to capture flow details. Since the primary focus is on observing

pressure changes within the hot channel, its grid is further refined to enhance resolution. Pressure wave peak values at points A, B2, and C2 are selected for comparative analysis as the grid number varies. Grid independence verification results are presented in Fig. 20 [FIGURE:20], showing that when the grid count reaches 860,000, the pressure peaks at all monitored points exhibit negligible variation with additional grid refinement. Consequently, this grid configuration is chosen for subsequent calculations, and the generated grid is visualized in Fig. 21 [FIGURE:21].

### B. The Effect of Specific Heat Capacity on Pressure Waves

As concluded in the previous section, the density of S-CO<sub>2</sub> is described using the PR equation of state. The viscosity and thermal conductivity are calculated using bilinear interpolation, where the physical properties are interpolated based on both temperature and pressure as the two parameters and then imported through UDF. This section examines the effects of pressure-dependent specific heat capacity variations on pressure wave propagation. Pressure wave analysis of the specific heat capacity of point A and B2 was conducted at temperatures ranging from 550 K to 800 K under the conditions of 0.1 MPa, 10 MPa and 20 MPa, as shown in Fig. 22 [FIGURE:22] and Fig. 23 [FIGURE:23].

The results indicate that specific heat capacity variations under the three pressures have negligible effects on pressure wave propagation, with nearly identical trends and peak values. This is because the operating temperature is in the high-temperature range, far from the pseudo-critical region, thereby minimizing the pressure effect on specific heat capacity. Thus, this study uses the specific heat capacity at 20 MPa for calculations.

### C. Pressure Analysis

Given that the sound speed in liquid lead-bismuth eutectic approaches 1900 m/s, pressure waves exhibit rapid propagation with short transit times. During boundary failure accidents, the most intense pressure wave dynamics occur in the initial stage, after which pressure gradually stabilizes over time. To ensure comprehensive observation of pressure wave propagation while managing computational costs, a long-time-scale simulation was first performed to identify the phase with the most intense pressure waves. Subsequently, short time-step simulations were conducted to characterize the fine-scale features of pressure wave propagation.

Monitoring the CO<sub>2</sub> volume fraction at points B and C, as shown in Fig. 26 [FIGURE:26], reveals that CO<sub>2</sub> starts to appear at point B around 0.001 s and at point C around 0.015 s, indicating CO<sub>2</sub> migration from the rupture to these locations. The pressure increase at this stage differs from the initial 0.001 s: it is not caused by the rupture-induced shockwave but rather by the gradual filling of the pipeline with released CO<sub>2</sub> gas, leading to pressure buildup.

### 1. Long Time Scale Simulation Fig. 24

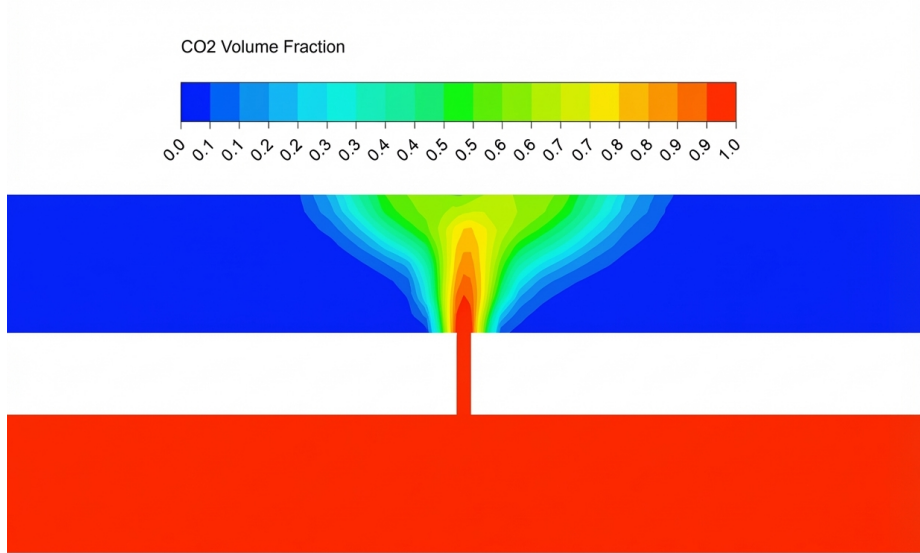


Figure 1: Figure 24

and Fig. 25 [FIGURE:25] show results performed with a time step of 1E-04 s. The pressure wave undergoes the most significant changes during the first 0.001 s, after which the pressure gradually stabilizes. Starting at approximately 0.015 s, the pressure at points B and C gradually increases. For the CO<sub>2</sub> channel, pressure changes can be considered negligible, remaining close to the operating pressure of 20 MPa. This is because the properties of supercritical fluids lie between liquid and gas, allowing it to fill the entire channel like a gas, while also exhibiting the flow characteristics of a liquid, resulting in good expansion properties. When leakage occurs, the incoming CO<sub>2</sub> at the inlet rapidly compensates for the loss. Additionally, due to the high operating pressure of CO<sub>2</sub>, pressure waves reflected back from the LBE channel are almost negligible.

The volume fraction of CO<sub>2</sub> at the hot channel inlet and outlet was monitored. As shown in Fig. 27 [FIGURE:27], CO<sub>2</sub> begins to appear at both locations after 0.015 s. Due to flow direction effects, the outlet exhibits CO<sub>2</sub> earlier than the inlet, indicating that flow-induced entrainment dominates over buoyancy-driven upward migration. Within the subsequent 0.02 s, the CO<sub>2</sub> volume fraction at both inlet and outlet rapidly increases to 90%, nearly filling the entire inlet and outlet. CO<sub>2</sub> completely fills the hot channel, demonstrating that during a PCHE boundary failure accident, CO<sub>2</sub> is highly likely to escape from the heat exchanger into the reactor system, posing a threat to reactor safety.

**2. Short Time Scale Simulation** Based on the long-timescale pressure wave analysis in the previous section, the most intense pressure wave variation occurs within the first 0.001 s after the accident initiation. Consequently, in this section, a short time step is used to specifically analyze the pressure wave propagation within 0.001 s. Long time scale calculations, compared to short time scale simulations as shown in Fig. 28 [FIGURE:28], omit many characteristics of pressure wave propagation, such as periodic pressure wave transmission phenomena analogous to shock tube behavior. The compression wave generated at the rupture propagates bidirectionally through the pipeline. Upon reaching the inlet and outlet boundaries, it reflects as expansion waves. These reflected expansion waves subsequently converge and superimpose at the pipeline's mid-section, forming a higher-amplitude combined expansion wave. Following this interaction, the expansion waves separate and continue propagating toward the boundaries, where they reflect again as compression waves. These compression waves then converge centrally, completing one full cycle. This iterative process continues, with pressure waves reflecting and superimposing throughout the pipeline until complete attenuation is achieved.

As shown in Fig. 29 [FIGURE:29], the pressure wave reaches point B2 at 0.08 ms, and by 0.24 ms, it has returned, completing one cycle. The time interval from one peak to another is approximately 0.2 ms, and the propagation time is consistent with that of sound propagation in LBE. But point A exhibits no pressure oscillations. This is because point A is positioned directly above the rupture point. After the pressure reaches its peak,  $\text{CO}_2$  gas rapidly fills the pipeline in the vicinity of point A. Thereafter, the pressure exhibits a linear change, primarily due to the depressurization of  $\text{CO}_2$ .

Fig. 30 [FIGURE:30] illustrates the pressure evolution in the cold channel. Regardless of whether the simulation uses a long or short time scale, pressure wave variations within the cold channel remain minimal. After the accident occurs, the pressure in the cold channel starts to decrease, but the reduction is negligible, and the pressure remains nearly constant at the operating pressure of 20 MPa. Notably, the cold channel pressure also exhibits periodic variations: after 2-3 oscillations, the pressure gradually stabilizes. The period of this periodic variation is approximately 1 ms, and the sound speed in S- $\text{CO}_2$  is about 400 m/s, which matches the theoretical calculation results. For monitoring points that are symmetrically located around the crack, such as B1, B2, C1, and C2, their propagation characteristics are almost identical, with negligible influence from the direction of fluid flow. Although using long time-step simulation calculations can reduce computational effort, the accuracy in terms of characteristics such as the propagation of pressure waves and peak values is far less precise compared to short time-step simulations. However, for observing trend changes, such as the variation in gas fractions within the pipeline or changes in pressure waves, long time-step calculations can fully meet the computational requirements.

Monitoring the pressure at rupture point R, as shown in Fig. 31 [FIGURE:31], revealed a sharp pressure drop within 0.1 ms, followed by a stable period lasting

approximately 0.25 ms, after which another decline occurs and the pressure eventually stabilizes at around 10 MPa. The duration of the first pressure stabilization phase is consistent with the transition period observed at point A. Further analysis of the temperature and velocity at point R (as shown in Fig. 32 [FIGURE:32]) reveals that these parameters exhibit similar variation trends to those at point R. A comparison of pressure, temperature, and velocity at point R with the pressure at point A is shown in Fig. 33 [FIGURE:33]. Both points had a stable period prior to 0.25 ms.

During the accident, the expansion of CO<sub>2</sub> could be divided into two types. Due to the rupture's perpendicular orientation relative to the flow path, supercritical carbon dioxide initially sprayed freely along the crack direction. Fig. 34 [FIGURE:34] presents the CO<sub>2</sub> volume fraction distribution on the rupture plane perpendicular to the flow direction at 0.03 ms. At this stage, the flow velocity is approximately 250 m/s, which remains below the local speed of sound (under 14 MPa, 595 K conditions), and critical flow conditions are not yet achieved. When the ejected CO<sub>2</sub> impacts the upper wall and is deflected, it fills the rupture plane and begins expanding laterally along the channel. Fig. 35 [FIGURE:35] shows the distribution of CO<sub>2</sub> volume fraction on the cross-sectional plane perpendicular to the flow direction at the breach location at 0.26 ms. Fig. 36 [FIGURE:36] illustrates the CO<sub>2</sub> volume fraction distribution on the rupture plane parallel to the flow direction at 0.26 ms. The CO<sub>2</sub> expands laterally along both sides of the flow channel, and all subsequent CO<sub>2</sub> leakage from the rupture follows this expansion pattern. By 1 ms, the leakage velocity stabilizes at approximately 360 m/s. As shown in Fig. 33, the temperature remains steady around 560 K, and the pressure maintains at 10 MPa. At this stage, the leakage velocity reaches the local sound speed, signifying that the CO<sub>2</sub> flow has reached critical flow conditions. With continuous CO<sub>2</sub> replenishment from the cold channel inlet, the depressurization process will persistently proceed under critical flow condition.

## V. Conclusion

This study decouples the interaction characteristics between S-CO<sub>2</sub> and lead-bismuth eutectic into two distinct models: a transcritical depressurization model and a liquid metal-gas contact model. These models are verified through corresponding experiments to demonstrate the feasibility of simulating the pressure boundary failure accident of printed circuit heat exchangers. ANSYS Fluent is used to simulate the boundary condition failure accident of the PCHE, and an analysis of pressure wave propagation in the pipeline is conducted. The results are summarized as follows:

1. Through experimental validation, the Peng-Robinson (PR) equation of state demonstrates excellent applicability in simulating the transcritical depressurization of S-CO<sub>2</sub>.
2. Turbulence model selection is critical for accurate simulation of supercriti-

cal CO<sub>2</sub> transcritical depressurization. By comparing several mainstream CFD turbulence models with experiments, the SST k- $\omega$  low-Re model is shown to significantly enhance prediction accuracy for CO<sub>2</sub> transcritical depressurization behavior.

3. In the pressure boundary failure accident of printed circuit heat exchangers, the injection of high-pressure S-CO<sub>2</sub> into low-pressure lead-bismuth eutectic (LBE) generates shock wave effects within the pipeline. The pressure wave exhibits quasi-periodic oscillations, reaching almost 17 MPa within 0.1 ms after the accident occurs and then gradually decays. By 10 ms, leaked CO<sub>2</sub> begins to fill the entire hot channel, causing renewed pressure rise due to CO<sub>2</sub> migration. At 30 ms, CO<sub>2</sub> concentration at the inlet/outlet reaches nearly 90%, indicating potential leakage into the reactor system.

This study focuses on the simulation of pressure boundary failure accidents for a single rupture size. Further investigation is required to examine the effects of varying rupture dimensions on accident progression, as well as the influence of rupture location on pressure wave dynamics and CO<sub>2</sub> migration within the pipeline. Additionally, the observed pressure wave characteristics exhibiting high peak magnitudes but short duration may induce structural failure in the heat exchanger. Stress analysis is required to assess the structural impact. These aspects need to be further researched in future studies.

## References

- [1] Pioro, I.L., Introduction: Generation Iv International Forum. HANDBOOK OF GENERATION IV NUCLEAR REACTORS, 2016.
- [2] Dawei, C., S. Lei and L. Jiming, Study on coupling heat transfer model and characteristics of supercritical carbon dioxide and liquid lead-bismuth eutectic. THERMAL POWER GENERATION, 2022. 51(6): p. 59-67.
- [3] Yike, N., et al., A review of lead-bismuth supercritical CO<sub>2</sub> heat transfer in lead-bismuth fast reactor-supercritical CO<sub>2</sub> cycle system. Electric Power Technology and Environmental Protection, 2023. 39(6): p. 471-483.
- [4] Eoh, J., et al., Potential sodium-CO<sub>2</sub> interaction of a supercritical CO<sub>2</sub> power conversion option coupled with an SFR: Basic nature and design issues. Nuclear Engineering and Design, 2013. 259: p. 88-101.
- [5] Kisohara, N., Y. Sakamoto and S. Kotake, Preliminary Conceptual Design of the Secondary Sodium Circuit-Eliminated JSFR (japan Sodium Fast Reactor) Adopting a Supercritical CO<sub>2</sub> Turbine System, 1; Sodium/CO<sub>2</sub> Heat Exchanger. 2014. 214: p. 1-33.
- [6] Jintao, L., et al., Corrosion Behavior of Alloys in Supercritical CO<sub>2</sub> Brayton Cycle Power Generation. Proceedings of the CSEE, 2016. 36(3): p. 739-745.

[7] Kang, L., The physical mechanism of the supercritical CO<sub>2</sub> leakage process in small scale laboratory conditions.. 2016, University of Science and Technology of China.

[8] Gebbeken, B. and R. Eggers, Blowdown of carbon dioxide from initially supercritical conditions. Journal of loss prevention in the process industries, 1996. 9(4): p. 285-293.

[9] Wang, J., et al., Study on Factors Affecting During Carbon Dioxide Vessel Decompression at Supercritical Pressure. Nuclear Science and Technology, 2021. 09: p. 29-37.

[10] Guo, X., et al., Pressure responses and phase transitions during the release of high pressure CO<sub>2</sub> from a large-scale pipeline. Energy, 2017. 118: p. 1066-1078.

[11] Yang, M., et al., Characteristic Analysis and Model Validation of Supercritical Carbon Dioxide Ejection in Pressure Vessel. Atomic Energy Science and Technology, 2023. 57(7): p. 1363-1372.

[12] Feng, L., Study on the leakage and diffusion behavior of supercritical pressure CO<sub>2</sub> from pipelines. 2016, Tsinghua University.

[13] Woolley, R.M., et al., Experimental measurement and Reynolds-averaged Navier-Stokes modelling of the near-field structure of multi-phase CO<sub>2</sub> jet releases. International Journal of Greenhouse Gas Control, 2013. 18: p. 139-149.

[14] Liao, S.M. and T.S. Zhao, Measurements of Heat Transfer Coefficients From Supercritical Carbon Dioxide Flowing in Horizontal Mini/Micro Channels. Journal of Heat Transfer, 2002. 124(3): p. 413-420.

[15] Ribert, G., et al., Simulation of supercritical flows in rocket-motor engines: application to cooling channel and injection system. Progress in Propulsion Physics 4, 2013: p. 205-226.

[16] Xianliang, L., et al., Research progress on conjugated heat transfer between supercritical carbon dioxide and liquid metals. THERMAL POWER GENERATION, 2023. 52(6): p. 1-11.

[17] Liu, J.P., et al., Experimentation and correlation of R744 two-phase flow through short tubes. Experimental Thermal and Fluid Science, 2004. 28(6): p. 565-573.

[18] Utili, M., et al., THALLIUM: An experimental facility for simulation of HCLL In-box LOCA and validation of RELAP5-3D system code. Fusion Engineering and Design, 2017. 123: p. 226-230.

[19] Shichao, Z., et al., Pressure Propagation Experiments of PbLi Impacted by High Pressure Helium under the Condition of Fracture. Nuclear Science and Engineering, 2019. 39(6): p. 651-656.

- [20] Shichao, Z., Transient Study of In-box LOCA in Dual-functional Lead Lithium Blanket. 2020, University of Science and Technology of China.
- [21] Alekseev, M.V., et al., Numerical simulation of pulsed gas-to-liquid injection modes using open source CFD software package OpenFoam. Journal of physics. Conference series, 2018. 1105(1): p. 12085.
- [22] ZHANG C, ECKERT S, GERBETH G. The flow structure of a bubble-driven liquid-metal jet in a horizontal magnetic field[J]. Journal of Fluid Mechanics, 2007,575:57-82.
- [23] Chong, Q., Numerical Simulation and Analysis of Steam Generator Tube Rupture Accident of Straight Tube Heat Exchanger in Lead-cooled Fast Reactor. 2024, University of Science and Technology of China.
- [24] Jiaming, C. and C. Hongli, Void Transport after Steam Generator Tube Leakage in Natural Circulation Lead-cooled Fast Reactor. Atomic Energy Science and Technology, 2020. 54(12): p. 2344-2352.
- [25] Usov, E.V., et al., Experimental and numerical simulation of gas bubbles motion in liquid metal. Journal of physics. Conference series, 2018. 1128(1): p. 12044.
- [26] Kefan. Z., et al., SUMMER: A small modular lead-bismuth-cooled fast reactor for mobile energy supply. Progress in Nuclear Energy, 2023. 164: p. 104860.

*Source: ChinaXiv — Machine translation. Verify with original.*